



## A filter-based system mimicking the particle deposition and penetration in human respiratory system for secondhand smoke generation and characterization

Weixing Hao, Kashala Fabrice Kapiamba, Varuni Abhayaratne, Shoaib Usman, Yue-Wern Huang & Yang Wang

To cite this article: Weixing Hao, Kashala Fabrice Kapiamba, Varuni Abhayaratne, Shoaib Usman, Yue-Wern Huang & Yang Wang (2022) A filter-based system mimicking the particle deposition and penetration in human respiratory system for secondhand smoke generation and characterization, *Inhalation Toxicology*, 34:7-8, 189-199, DOI: [10.1080/08958378.2022.2075493](https://doi.org/10.1080/08958378.2022.2075493)

To link to this article: <https://doi.org/10.1080/08958378.2022.2075493>



Published online: 18 May 2022.



Submit your article to this journal [↗](#)



Article views: 67

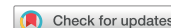


View related articles [↗](#)




View Crossmark data [↗](#)

RESEARCH ARTICLE



## A filter-based system mimicking the particle deposition and penetration in human respiratory system for secondhand smoke generation and characterization

Weixing Hao<sup>a</sup>, Kashala Fabrice Kapiamba<sup>a</sup>, Varuni Abhayaratne<sup>a</sup>, Shoaib Usman<sup>b</sup>, Yue-Wern Huang<sup>c</sup> and Yang Wang<sup>a</sup> 

<sup>a</sup>Department of Civil, Architectural and Environmental Engineering, Missouri University of Science and Technology, Rolla, MO, USA;

<sup>b</sup>Department of Nuclear Engineering and Radiation Science, Missouri University of Science and Technology, Rolla, MO, USA; <sup>c</sup>Department of Biological Sciences, Missouri University of Science and Technology, Rolla, MO, USA

### ABSTRACT

**Introduction:** Secondhand smoke endangers both the environment and the health of nonsmokers. Due to the scarcity of repeatable data generated by human subjects, a system capable of generating representative secondhand smoke is essential for studying smoke properties. This work presents the design and validation of a filter-based system that could mimic the particle deposition and penetration in human respiratory system for secondhand smoke generation and characterization.

**Methods:** Guided by our study on characterizing size-dependent filtration efficiency of common materials, we identified three filter media that generate similar particle deposition efficiencies compared to different regions of the human respiratory system over a wide submicron size range. We demonstrated the performance of the proposed filter-based system using various operating conditions. Additionally, we compared the properties of secondhand smoke particles to those of primary smoke particles.

**Results:** The difference in aerosol deposition efficiencies between the filter-based system and the International Commission on Radiological Protection (ICRP) model was less than 10% in the size range of 30 to 500 nm. High concentrations of metals were detected in the secondhand smoke. The contents of Ni and Cr generated from the secondhand electronic cigarettes are at least 20 and 5 times above the regulated daily maximum intake amount.

**Conclusion:** Given the agreement in aerosol respiratory deposition between the filter-based system and the ICRP model, such a system can facilitate laboratory studies of secondhand smoke due to its simple structure, high repeatability, and ease of control while remaining free of human subjects.

### ARTICLE HISTORY

Received 19 October 2021

Accepted 3 May 2022

### KEYWORDS

Respiratory deposition;  
secondhand smoke;  
electronic cigarette;  
aerosol; filter

### Introduction

Although the usage of cigarettes (such as tobacco and electronic cigarettes) is a lifestyle choice for smokers, secondhand smoke can be generated from these devices and pose involuntary health and environmental impact on nonsmokers, necessitating the characterization and quantification of these adverse effects (Andreoli et al. 2003; Office of the Surgeon General 2006; US Department of Health and Human Services 2014). However, this secondhand smoke, especially that directly generated from the exhalation of the cigarette users (e.g. when using electronic cigarettes), remains mostly understudied. Limited number of studies on secondhand electronic cigarette aerosols involved human subjects using the products and exhaling the smoke into a chamber or a sample collection device to analyze the smoke (Schripp et al. 2013; Czogala et al. 2014; Logue et al. 2017; Protano et al. 2017; Zhao et al. 2017; Kaufman et al. 2018;

Son et al. 2020), providing relatively accurate measurements of secondhand smoke exhaled by real smokers with wide ranges of ages, physical conditions, and smoking habits. However, conducting such studies involves complex human subject compliance and a significant number of variables, thereby limiting the amount of repeatable data that can be generated from the studies. Therefore, a simulated respiratory system that generates representative and consistent secondhand smoke will be substantial for studying the physical, chemical, and toxicological properties of the smoke.

The secondhand (exhaled) smokes are different from primary (inhaled) mainly due to the physical processes in the human respiratory system. As the smoke particles enter the respiratory system, they deposit on epithelial cells through inertial impaction, interception, Brownian diffusion, and gravitational settling mechanisms, each playing a different role in capturing particles of various size ranges (Hinds

1999). Additionally, particles of specific sizes would have different deposition efficiencies in the extrathoracic (ET), tracheobronchial (TB), and alveolar (AL) respiratory airways due to variations in the structure, air flow rate, and particle residence time (Heyder et al. 1986). As a result of particle deposition in the respiratory system, secondhand smoke would have a smaller number-based size distribution compared to primary smoke. To recapitulate the size-dependent deposition efficiency, the International Commission on Radiological Protection (ICRP) developed a human respiratory tract model that describes the deposition fractions in different regions of the respiratory system (Bair 1995). The most commonly used particle deposition fractions modeled by the ICRP assume that particles are composed of sodium chloride (NaCl). However, it was also noted that the composition of particles affected their respiratory deposition (ICRP 1995). In addition to semi-empirical models, advanced numerical models based on computational fluid dynamics (CFD) have also been developed to examine particle deposition in the respiratory system, as comprehensively reviewed in (Rostami 2009), with the majority of models addressing the oronasal and upper respiratory tracts only.

Apart from particle deposition, hygroscopic growth of particles is also needed to be considered. It is now recognized that during inhalation and exhalation, aerosols grow under high relative humidity (RH close to 99.5%) (ICRP 1995), and the growth rate is dependent on the hygroscopicity of the particle. This growth would have a profound impact on the fate of the secondhand smoke aerosols as their size distributions will be different from those of the primary smoke generated by conventional and electronic cigarettes. The inclusion of aerosol hygroscopic growth added significant complexity to the particle dynamics within the respiratory tract (Morrow 1986). The hygroscopic growth of particle size will affect the deposition efficiencies in the respiratory system, as shown in the study of the human respiratory deposition of biomass burning smoke (Löndahl et al. 2008). Modeling studies also found that the hygroscopic growth rates are higher for electronic cigarette aerosols than for tobacco cigarette aerosols. The effect of particle growth on deposition leads to a lower total deposition in the case of tobacco cigarette aerosols than for the electronic cigarette aerosols (Pichelstorfer et al. 2016). According to another modeling study, the inhalation of warm saturated air may also significantly grow the inhaled smoke aerosols, highlighting the impact of condensational growth in smoke aerosol deposition (Worth Longest and Xi 2008). In addition to hygroscopic growth, the phase change of the smoke particles due to volatile organics in the particles may further complicate the particle deposition in the respiratory system (Pankow 2001; Pichelstorfer et al. 2013; Zhang et al., 2013; Pichelstorfer and Hofmann 2015). Modeling studies show that medium-to-high soluble vapors have very high deposition values in the human upper airways, while insoluble species may penetrate further and deposit in deeper lung regions. Vapor deposition is also strongly influenced by the puffing behavior (Zhang and

Kleinstreuer 2011; Zhang et al. 2012). As for cigarette aerosols, most of the nicotine is deposited by the vapor phase for both electronic and tobacco cigarettes (Pichelstorfer et al. 2016).

In order to generate representative secondhand smoke aerosols, a simulated respiratory system needs to mimic the size-dependent particle deposition pattern, hygroscopic growth, as well as the phase change of smoke particles. Previous studies show that the upper respiratory tract (mouth-throat and upper tracheobronchial regions) can be simulated with cast and 3D-printed structures, which can be used to imitate the realistic particle deposition and hygroscopic growth under the high RH environment (Hindle and Longest 2010; Zhou et al. 2011; Xi et al. 2013; Chen et al. 2017). The mouth-throat model with NaCl particles under humidified conditions shows that a high relative humidity inlet can substantially enhance the average growth ratio of hygroscopic droplets (Chen et al. 2017). Recently, a more realistic human respiratory tract containing lower tracheobronchial regions was manufactured, representing physiological thermal conditions in the human lungs (Asgari et al. 2019, 2021), however, the particle deposition efficiencies have not been experimentally determined. Until now, no systems have been available for simulating the particle deposition in the alveolar regions due to the requirement of a large surface area for particle deposition through Brownian diffusion, which cannot be achieved with cast and 3D-printed structures. Moreover, due to the strong dependence of vapor adsorption and absorption on the properties of the deposited surfaces, no studies examined vapor deposition in such simulated respiratory systems (Hindle and Longest 2010; Zhou et al. 2011; Xi et al. 2013; Nordlund et al. 2017; Asgari et al. 2019, 2021).

Guided by our recent studies on characterizing size-dependent filtration efficiency of common household fabric materials (Hao et al. 2020, 2021), we identified several standardized filter media that are capable of generating nearly identical particle deposition efficiencies modeled by the ICRP in various regions of the human respiratory system over a wide submicron size range under the relative humidity of 90%. It is thus feasible to assemble these filter media to construct a simulated human respiratory system that can mimic aerosol deposition and generate representative secondhand smoke, assuming particle deposition follows that of NaCl particles used in the ICRP. The hygroscopic growth of the particles can be achieved by mixing the sampled smoke with a stream of humidified air. Such a system can greatly enhance the capacity to predict the toxicological profile of cigarette aerosols due to its simple structure, high repeatability, and ease of control while remaining free of human subjects. In this study, we first examined and compared the particle deposition mechanisms in the human respiratory system and filter media, and then validated the performance of such a filter-based simulated respiratory system under various sampling flow rates and relative humidities. We further generated secondhand smoke particles from tobacco and electronic cigarettes and compared their properties against primary smoke particles.

## Methods

### Particle deposition mechanisms in the human respiratory system and filter media

The human respiratory system consists of the extrathoracic (ET), tracheobronchial (TB), and alveolar (AL) regions. The transport and deposition of particles onto airway surfaces are governed by Brownian diffusion, inertial impaction, interception, and gravitational settling. Particle deposition onto different regions of the respiratory system depends on the aerodynamic size of the particle ( $d_{ae}$ ), air flow rate ( $Q$ ), residence time in the alveolar region ( $t_A$ ), residence time in the alveolar region ( $t_B$ ), and the tidal volume ( $V$ ). (Heyder et al. 1986) calculated the theoretical particle deposition efficiency in different sub-regions of the human respiratory system, including the nasal passage ( $e_N$ ), larynx ( $e_L$ ), upper bronchial airways ( $e_{UB}$ ), lower bronchial airways ( $e_{LB}$ ), and alveolar region ( $e_{AL}$ ) as follows:

$$e_N = 1 - 1/(0.00033d_{ae}^2 Q + 1) \quad (1)$$

$$e_L = 1 - 1/((0.00009d_{ae}^2 Q^{0.66} V^{-0.25})^{1.5} + 1) \quad (2)$$

$$e_{UB} = 1 - \exp(-(0.0000265d_{ae}^2 Q)^{1.6}) \quad (3)$$

$$e_{LB} = 1 - \exp(-(0.018d_{ae}^2 t_B)^{1.4}) \quad (4)$$

$$e_{AL} = 0.2(d_{ae}^2 t_A)^{0.6} \quad (5)$$

With the particle deposition efficiency in each region of the respiratory system, the total deposition can be estimated by calculating the theoretical particle deposition fraction penetrating the entire system, summarized in Heyder et al. (1986). Figure 1 shows the human respiratory deposition efficiency ( $\eta_{Tot}$ ) calculated using the method of deposition

of unit density spheres in the respiratory tract during nasal breathing as a function of particle size and breathing pattern ( $750 \text{ cm}^3 \text{ s}^{-1}$  mean flow rate; 4 s breathing cycle period;  $1500 \text{ cm}^3$  tidal volume). The total deposition shows a 'U' shape, since smaller particles are more likely to be removed by Brownian diffusion, and larger particles are more likely to be removed by interception, impaction, and gravitational settling.

Similar to the human respiratory system, fibrous filters composed of non-electret fiber materials also collect particles using the Brownian diffusion, interception, impaction, and gravitational settling mechanisms (Hinds 1999). The overall particle removal efficiency of a filter,  $\eta_f$ , can be determined by

$$\eta_f = 1 - \exp\left(\frac{-4\alpha E_\Sigma t}{\pi D_f}\right) \quad (6)$$

where  $\alpha$  is the volume fraction of fibers,  $E_\Sigma$  is the total single-fiber efficiency,  $t$  is the thickness of the fiber,  $D_f$  is the fiber diameter. Each of the deposition mechanisms contributing to  $E_\Sigma$  is described below.

Collection by interception occurs when a particle follows a gas streamline that happens to come within one particle radius of the surface of a fiber. The single-fiber efficiency due to interception depends on the dimensionless parameter  $R$ .

$$R = \frac{D_p}{D_f} \quad (7)$$

where  $D_p$  is particle diameter. The single-fiber efficiency for interception,  $E_R$ , is given by (Lee and Ramamurthi 1993),

$$E_R = \frac{(1-\alpha)R^2}{Ku(1+R)} \quad (8)$$

where  $Ku$  is the Kuwabara hydrodynamic factor, a dimensionless factor that compensates for the effect of distortion of the flow field around a fiber because of its proximity to other fibers.  $Ku$  depends only on the volume fraction of fibers in a filter,  $\alpha$ .

$$Ku = -\frac{\ln\alpha}{2} - \frac{3}{4} + \alpha - \frac{\alpha^2}{4} \quad (9)$$

Inertial impaction of a particle on a fiber occurs when the particle, because of its inertia, is unable to adjust quickly enough to the abruptly changing streamlines near the fiber and crosses those streamlines to hit the fiber. The parameter that governs this mechanism is the Stokes number ( $Stk$ ), as the ratio of particle stopping distance to fiber diameter.

$$Stk = \frac{\tau U_0}{D_f} = \frac{\rho_p D_p^2 C_c U_0}{18\eta D_f} \quad (10)$$

where  $U_0$  is the face velocity. The single-fiber efficiency for impaction,  $E_I$ , is given by (Yeh and Liu 1974),

$$E_I = \frac{(Stk)J}{2Ku^2} \quad (11)$$

where  $J = (29.6 - 28\alpha^{0.62})R^2 - 27.5R^{2.8}$  for  $R < 0.4$ . Impaction is the most important mechanism for large particles.

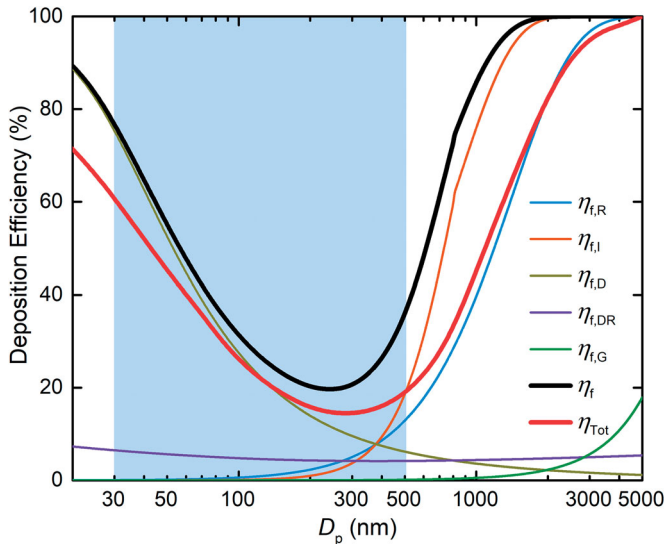


**Figure 1.** Particle deposition efficiencies due to different mechanisms and total efficiency in a filter with a fiber diameter ( $D_f = 5 \mu\text{m}$ ), a thickness ( $t = 1 \text{ mm}$ ), volume fraction of fibers ( $\alpha = 0.05$ ), and a face velocity ( $U_0 = 0.1 \text{ m/s}$ ), and a comparison against the particle deposition efficiencies in the human respiratory system. The shaded area shows the submicron size range of interest in this study.  $\eta_{f,R}$ ,  $\eta_{f,I}$ ,  $\eta_{f,D}$ ,  $\eta_{f,DR}$ ,  $\eta_{f,G}$  stand for filter efficiency for interception, impaction, diffusion, diffusion-interception interaction, gravitational settling mechanisms, respectively.  $\eta_f$  stands for total filter efficiency,  $\eta_{Tot}$  stands for total particle deposition efficiencies in the human respiratory system.

The Brownian motion of small particles is sufficient to greatly enhance the probability of their hitting a fiber while traveling past it on a nonintercepting streamline. The single-fiber efficiency for diffusion,  $E_D$ , is a function of the dimensionless Peclet number (Pe),

$$Pe = \frac{D_f U_0}{D} \quad (12)$$

where  $D$  is the particle diffusion coefficient.  $E_D$  is given by

$$E_D = 2Pe^{-2/3} \quad (13)$$

In estimating the overall single-fiber collection efficiency near the size of minimum efficiency, it is necessary to include an interaction term to account for enhanced collection due to interception of the diffusing particles,

$$E_{DR} = \frac{1.24R^{2/3}}{(Ku Pe)^{1/2}} \quad (14)$$

The dimensionless number that controls deposition due to gravitational settling is  $G$

$$G = \frac{V_{TS}}{U_0} = \frac{\rho_g D_p^2 C_g}{18\eta U_0} \quad (15)$$

The single-fiber efficiency for gravitational settling,  $E_G$ , is given by

$$E_G \approx G(1 + R) \quad (16)$$

The mechanical single-fiber efficiencies are correctly combined by

$$E_\Sigma = 1 - (1 - E_R)(1 - E_I)(1 - E_D)(1 - E_{DR})(1 - E_G) \quad (17)$$

One can calculate the filter particle removal efficiency  $\eta_{f,R}$ ,  $\eta_{f,I}$ ,  $\eta_{f,D}$ ,  $\eta_{f,DR}$ ,  $\eta_{f,G}$  for the interception, impaction, diffusion, diffusion-interception interaction, gravitational settling mechanisms separately with Equations (6) to (17) (although normal filters cover several or all of the mechanisms), and an example plot is shown in Figure 1, assuming  $D_f = 5 \mu\text{m}$ ,  $t = 1 \text{ mm}$ ,  $\alpha = 0.05$ , and  $U_0 = 0.1 \text{ m/s}$ . It can be observed that the particle deposition efficiencies in filters follow a similar trend compared to those in the human respiratory system ( $\eta_{Tot}$ ). It is therefore, feasible, to construct a filter-based simulated respiratory system that regenerates the particle deposition patterns in the human respiratory system for producing secondhand smoke. In this study, due to the importance of submicron particles in cigarette smoke aerosols and the limited size range of the instrument measuring aerosol size distributions, we focus on the size range from 30 to 500 nm.

### Identifying the filters for the simulated respiratory system

The proposed simulated system is composed of five sets of filters, each representing a region of the human respiratory system (Figure 2). To simulate the passage of air flow during breathing, the first and fifth filters mimic the ET region, the second and fourth filters mimic the TB region, and the

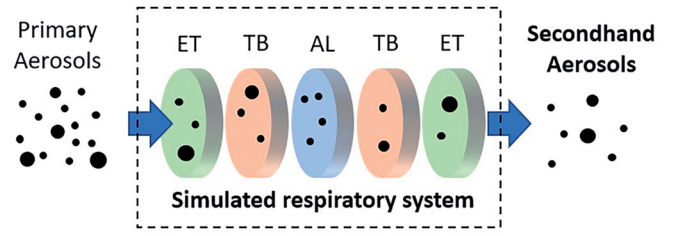


Figure 2. A schematic diagram of the filter-based simulated respiratory system composed of five filters in tandem. ET, TB, and AL stand for extrathoracic, tracheobronchial, and alveolar regions.

third filter in the middle of the system mimics the AL region. The smoke is inhaled through ET, TB, AL regions, and then exhaled through TB, ET regions, respectively. To simulate the particle deposition in the human respiratory system, the particle deposition efficiency (or the filtration efficiency of particles) through the filter material should satisfy the ICRP model under the humidity relevant to human lung conditions. Assuming that the filtration efficiency of the filter materials used for the ET, TB, and AL regions are  $\eta_{f,ET}$ ,  $\eta_{f,TB}$ , and  $\eta_{f,AL}$ , and the particle deposition fractions in the ET, TB, and AL regions in the ICRP model are  $\eta_{ET}$ ,  $\eta_{TB}$ , and  $\eta_{AL}$ , we can construct Equations (18) to (20) to relate the wholistic deposition efficiencies in ET, TB, and AL to the specific filter deposition efficiencies. Note that particles deposit on the ET and TB filters both upstream and downstream of the AL filter. Therefore, we used deposition fraction ( $\eta_{ET}$ ,  $\eta_{TB}$ ,  $\eta_{AL}$ ) to refer to the fraction of particles deposited in a specific region of the respiratory system through the entire inhalation and exhalation process; we used deposition efficiency ( $\eta_{f,ET}$ ,  $\eta_{f,TB}$ ,  $\eta_{f,AL}$ ) to refer to the fraction of particles deposited when air flow passes through a specific region in a one-time process. Considering the air flow and particle transport and treating each region of the respiratory system as a filter media, the deposition fractions and deposition efficiencies are related by

$$\eta_{ET} = \eta_{f,ET} + \eta_{f,ET}(1 - \eta_{f,AL})(1 - \eta_{f,ET})(1 - \eta_{f,TB})^2 \quad (18)$$

$$\eta_{TB} = \eta_{f,TB}(1 - \eta_{f,ET}) + \eta_{f,TB}(1 - \eta_{f,AL})(1 - \eta_{f,ET})(1 - \eta_{f,TB}) \quad (19)$$

$$\eta_{AL} = \eta_{f,AL}(1 - \eta_{f,ET})(1 - \eta_{f,TB}) \quad (20)$$

$\eta_{f,ET}$ ,  $\eta_{f,TB}$ ,  $\eta_{f,AL}$ ,  $\eta_{ET}$ ,  $\eta_{TB}$ , and  $\eta_{AL}$  are dependent on particle size ( $D_p$ ), where  $\eta_{ET}$ ,  $\eta_{TB}$ , and  $\eta_{AL}$  also satisfy the following equations according to the ICRP model (Hussain et al. 2011; Wang et al. 2017).

$$\eta_{ET} = IF \left[ \frac{1}{1 + \exp(6.84 + 1.183 \ln D_p)} + \frac{1}{1 + \exp(0.924 - 1.885 \ln D_p)} \right] \quad (21)$$



$$\eta_{\text{TB}} = \frac{0.00352}{D_p} \left\{ \exp \left[ -0.234(\ln D_p + 3.40)^2 \right] + 63.9 \exp \left[ -0.819(\ln D_p - 1.61)^2 \right] \right\} \quad (22)$$

$$\eta_{\text{AL}} = \frac{0.0155}{D_p} \left\{ \exp \left[ -0.416(\ln D_p + 2.84)^2 \right] + 19.11 \exp \left[ -0.482(\ln D_p - 1.362)^2 \right] \right\} \quad (23)$$

$$\text{IF} = 1 - 0.500 \left( 1 - \frac{1}{1 + 0.000760 D_p^2} \right) \quad (24)$$

where  $D_p$  is in micrometers, and IF is the inhalable fraction. The filtration efficiencies of the filter media ( $\eta_{\text{f,ET}}$ ,  $\eta_{\text{f,TB}}$ , and  $\eta_{\text{f,AL}}$ ) can be obtained by solving Equations (18) to (20) using the non-linear solver in MATLAB<sup>®</sup>. Filter materials that have filtration efficiencies approximating the values of  $\eta_{\text{f,ET}}$ ,  $\eta_{\text{f,TB}}$ , and  $\eta_{\text{f,AL}}$  are ideal candidates for the simulated respiratory system. Note that in Eqs. (18) to (20), we treated each ET, TB, and AL region as a filter media, which differs from the actual human respiratory system with time-dependent aerosol transport and deposition. However, with the appropriate filter media, the filter-based system can achieve a similar particle deposition fraction compared to the human respiratory system, which can be used to simulate particle deposition and generate representative secondhand smoke.

In our previous studies (Hao et al. 2020, 2021), a wide range of common materials were evaluated in their size-dependent filtration efficiencies with the experimental setup shown in Supplementary Figure S1, and we managed to identify three different types of filter media that have filtration efficiencies approaching  $\eta_{\text{f,ET}}$ ,  $\eta_{\text{f,TB}}$ , and  $\eta_{\text{f,AL}}$  (see Supplementary Information). The selected filter media are then assembled according to Figure 2 to form a filter-based simulated respiratory system, and the particle deposition efficiency is determined and compared against the ICRP model, which is calculated using

$$\eta_{\text{Tot}} = \text{IF} \left[ 0.0587 + \frac{0.911}{1 + \exp(4.77 + 1.49 \ln D_p)} + \frac{0.943}{1 + \exp(0.508 - 2.58 \ln D_p)} \right] \quad (25)$$

Test aerosols, including the NaCl generated by the nebulizer, tobacco cigarette smoke, and electronic cigarette smoke, are introduced to the filter-based system for size distribution characterizations. The aerosol flow was conditioned in their RH by mixing the generated aerosols with filtered humidified air, reaching a final RH of  $90 \pm 5\%$  (see Supplementary Information). A high RH value of 99.5% in the ICRP (Ferron 1977; Blanchard and Willeke 1984; Tu and Knutson 1984; Anselm et al. 1986; ICRP 1995) could not be achieved with the experimental setup, because (1) there are difficulties in maintaining the RH near saturation, since a temperature fluctuation of  $1^\circ\text{C}$  at  $23^\circ\text{C}$  would result in an RH fluctuation of more than 5% near saturation, and (2) there are limitations of the aerosol measuring instrument (can only sample aerosols with RH below 95%). However, at 90% RH, the deliquescence points of most common salts have been reached (Seinfeld and Pandis 2008), and the deposition patterns should not be

significantly different from those under 99.5% due to the limited size change after deliquescence. The previous study (Ferron et al. 1988) showed that uncertainties in the RH values in the upper human airways have some effects on particle growth, but less than 2% on particle deposition. The tobacco smoke aerosols are generated by the research reference cigarette (1R6F, University of Kentucky, KY), and the electronic cigarette aerosols are generated from the VOOPOO (Drag X, Shenzhen Woody Vapes Technology Co, China) operated at a power of 40 W. Tobacco cigarette aerosols are generated by pulling airflow through the filter tip in the setup, and electronic cigarette smoke can be generated by clicking the activation button and then pulling from the downstream of the filter-based system. The aerosols from the tobacco and electronic cigarettes are sampled according to the standardized puff profile (2 s puff duration and 35 ml puff volume) (ISO 2000), and then introduced to a mixing chamber before they pass through the filter-based system. The size-dependent particle number concentrations for tobacco and electronic cigarette aerosols were tested at least three times. The size-dependent deposition efficiency was calculated by particle number concentrations at the downstream and upstream of the filter-based system. The standard deviations of the size distributions were used to calculate the size-dependent deposition efficiency standard deviation (see Supplementary Information).

### Measuring the metal contents in secondhand smoke aerosols

The filter-based system enables the direct sampling of the secondhand smoke aerosols for chemical composition analysis. Here we installed a Teflon filter (37 mm, SKC Inc.) downstream of the filter-based simulated respiratory system to collect the secondhand aerosols when the tobacco (1R6F), JUUL (JUUL Labs, Inc., Washington D.C., US), and VOOPOO, are used as the source of primary aerosols. Thirty puffs of aerosols are collected using the standardized puff profiles. Upon sample collection, the filters are digested with 70% nitric acid (Sigma-Aldrich, St. Louis, MO) in a digester block at  $95^\circ\text{C}$ , centrifuged, and mixed with 1% nitric acid into 10 ml solutions for analysis. The metal contents are quantified with the inductively coupled plasma-mass spectrometry (NexION 350 ICP-MS, PerkinElmer Inc., Waltham, MA, USA). Certified Trace Metals Quality Control Standard (QCI-034-1, NSI Lab Solutions, Raleigh, NC) was used as a control for all cation analyses performed for this study. All of the detailed configuration and method parameters of the ICP-MS can be found in our recent publication (Kapiamba et al. 2022).

## Results

### Size-dependent deposition efficiency of the filter-based simulated respiratory system

Among the materials tested, we found that two layers of Thai silk type A, four layers of Thai silk type B, and two layers of knit polyester have filtration efficiencies close to

those of the ET, TB, and AL regions ( $\eta_{f,ET}$ ,  $\eta_{f,TB}$ , and  $\eta_{f,AL}$ ) under the relative humidity of 90% (Figure 3), which are derived from the ICRP model (detailed in the Methods section). The properties of the filter media, such as grams per square meter (GSM), fiber diameter, and vendor information, are shown in Table 1, and the microscopic images of the filter medium are shown in Figure 3. The identified filter media were then assembled to construct the simulated respiratory system as indicated in Figure 2. From the particle deposition efficiencies (Figure 3), we can observe a higher particle deposition efficiency for particles below 50 nm ( $>40\%$ ), and enhanced deposition efficiencies for particles above 300 nm, which are resulted from the particle capture in the simulated AL and ET regions. On average, the absolute difference in aerosol deposition efficiencies between the filter-based simulated respiratory system and the ICRP model was below 10% in the size range of 30 to 500 nm. Although the filter-based system with the proposed filter materials does not consider the operation outside the range of human inhalation conditions established by the ICRP, given the similarities in the particle deposition mechanisms (Figure 1), new filter materials or new flow conditions can be selected to simulate the human respiratory system under different inhalation conditions. Collectively, such a system can be used to simulate particle deposition in the human respiratory system and the production of secondhand aerosols.

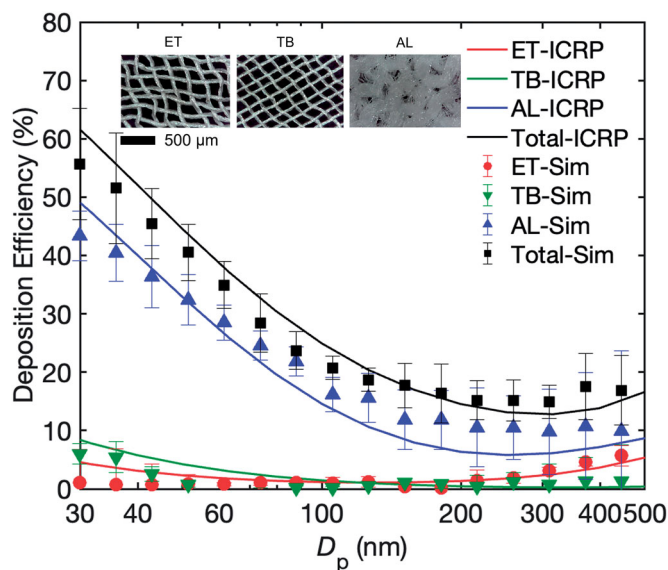


**Figure 3.** Size-dependent NaCl aerosol deposition efficiencies of the fabric materials simulating the extrathoracic region (ET), tracheobronchial region (TB), alveolar region (AL), and the entire (Total) human respiratory systems (markers), and the comparison to the theoretical deposition efficiencies (curves) derived from the ICRP model.

**Table 1.** Information on the fabric materials and the tests conducted.

Filter type	Brand	Fiber Diameter	Layers	GSM (g/m <sup>2</sup> )
Silk A	Thaisilks.com	125 $\mu$ m	2	76.05
Silk B	Thaisilks.com	90 $\mu$ m	4	72.09
Polyester	lfabric.com	230 $\mu$ m	2	105.44

Note: GSM stands for grams per square meter.

### Performance of the filter-based simulated respiratory system under different flow rates

We noted that the size-dependent particle deposition efficiencies in the ICRP model used in this study were obtained under the condition of an adult, nose-breathing male during light exercise (Hinds 1999; Hoover et al. 2007). Depending on factors such as age, posture, and other personal attributes, the respiratory flow rate may vary widely among individuals (Hinds 1999; Grinshpun et al. 2009), and the flow rate can influence the particle deposition accordingly. Therefore, we also examined the performance of the filter-based system under 50% and 150% of the default flow rate (which is assumed to be the breathing rate of a reference man  $1.2 \text{ m}^3 \text{ h}^{-1}$ ). The size-dependent particle deposition efficiencies through the combined filter-based simulated respiratory system and the comparison against the ICRP model are shown in Supplementary Figure S2. Generally, a higher flow rate leads to an enhanced particle deposition for particles above 200 nm and a reduced particle deposition for particles below 50 nm. The reduced deposition of the smaller particles under a higher flow rate originates from the shortened residence time of particles in the filter media, where the particles would have a lower probability of being captured by the filter. The greater deposition of larger particles under a higher flow rate results from the increased particle inertia and enhanced particle capture by impaction and interception. However, we should also note that the change of the size-dependent particle deposition is not significant, where the absolute difference of particle deposition efficiency is below 20%. Similar features in particle deposition can be observed in each region of the filter-based system (Supplementary Figure S3).

### Secondhand smoke generation with the filter-based simulated respiratory system

The assembled filter-based simulated respiratory system was then used to generate secondhand smoke aerosols, where an electronic cigarette (VOOPOO) and a tobacco research cigarette (1R6F) were used as the sources of primary aerosols. The size distributions of the primary and secondhand aerosols that were measured upstream and downstream of the filter-based system are shown in Figure 4, with NaCl aerosols used as a reference.

The mode diameters of the primary aerosols generated from the electronic and tobacco cigarettes are both approximately 300 nm, whereas the electronic cigarette generated a higher concentration of aerosols ( $2.5 \times 10^5 \text{ cm}^{-3}$ ) compared to that ( $8.0 \times 10^4 \text{ cm}^{-3}$ ) of the tobacco cigarette. Note that the size distributions of primary electronic and tobacco cigarette aerosols extended beyond 500 nm, which were not measurable with the instrument. Assuming that both the primary electronic cigarette and tobacco cigarette aerosols follow log-normal size distributions, we can estimate that the total concentrations of the electronic and tobacco cigarette aerosols are  $3.0 \times 10^5 \text{ cm}^{-3}$  (geometric mean diameter  $D_{pg} = 347 \text{ nm}$ , geometric standard deviation  $\sigma_g = 1.79$ ) and  $9.2 \times 10^4 \text{ cm}^{-3}$  ( $D_{pg} = 332 \text{ nm}$ ,  $\sigma_g = 1.75$ ), respectively. We

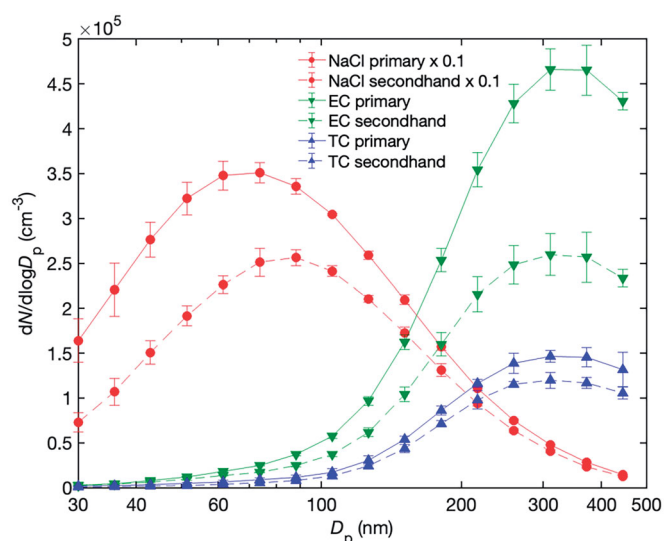


**Figure 4.** Size distributions of NaCl, VOOPOO electronic cigarette (EC), and tobacco cigarette (TC) aerosols upstream (primary) and downstream (secondhand) of the filter-based simulated respiratory system.

observe that the secondhand electronic and tobacco cigarette aerosols generated from the filter-based system show considerable changes in the size distributions compared to the corresponding primary aerosols. Although a fraction of primary aerosols is captured by the filter-based system, a considerable number of secondhand aerosols can still be emitted. For example, the total concentrations of secondhand electronic and tobacco cigarette aerosols in the 30 to 500 nm size range are  $1.5 \times 10^5$  and  $6.1 \times 10^4 \text{ cm}^{-3}$ , respectively. The concentrations become  $1.7 \times 10^5 \text{ cm}^{-3}$  ( $D_{pg} = 329 \text{ nm}$ ,  $\sigma_g = 1.80$ ) and  $7.4 \times 10^4 \text{ cm}^{-3}$  ( $D_{pg} = 326 \text{ nm}$ ,  $\sigma_g = 1.73$ ), respectively, by including particles above 500 nm and assuming that the secondhand aerosols follow log-normal size distributions. The total particle deposition efficiencies for electronic and tobacco cigarette aerosols are 39.5% and 23.9% based on size distributions below 500 nm, and 43.6% and 20.4% based on log-normal size distributions. However, we should also note that according to the ICRP lung model, the total deposition is not as important as where the aerosols are deposited, because the transfer of the aerosols to blood is not uniform from each compartment of the lung. Using the size distributions of aerosols upstream and downstream of the filter-based system, we also derived the size-dependent particle deposition efficiency for NaCl, electronic cigarette, and tobacco cigarette aerosols, which is shown in Figure 5. The relatively large deviation in particle deposition efficiency for electronic cigarette aerosols is due to the phase state of the particles, which can be explained by the dynamics of aerosol transport and evaporation that also occurs in human lungs. Further discussion can be found in the Discussion section.

#### Metal contents in secondhand smoke aerosols

With the filter-based simulated respiratory system, we collected the secondhand tobacco and electronic cigarette smoke, analyzed the heavy metal contents in these particles,

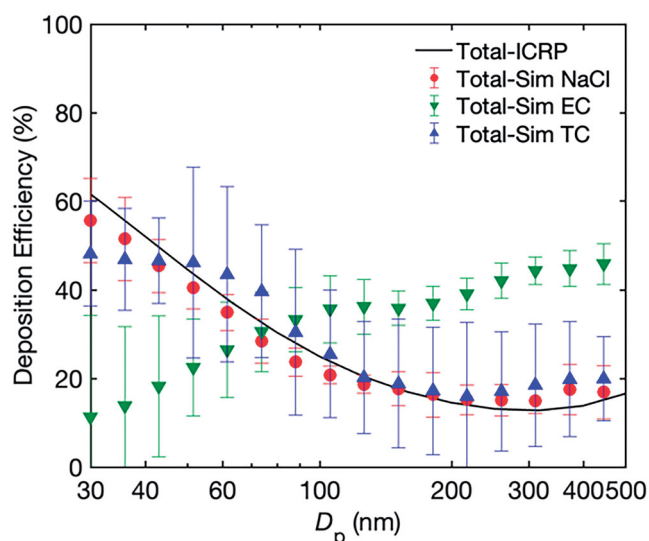


**Figure 5.** Size-dependent aerosol deposition efficiencies in the filter-based simulated respiratory system for NaCl, VOOPOO electronic cigarette (EC), tobacco cigarette (TC) aerosols, and comparison against the ICRP model.

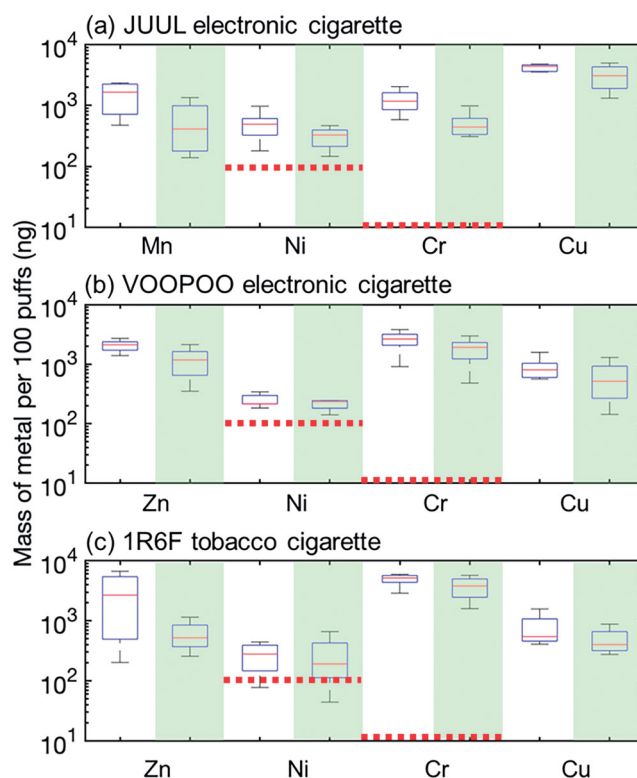


**Figure 6.** Mass of major metals (Mn, Zn, Ni, Cr, and Cu) for every 100 puffs of (a) JUUL electronic cigarette, (b) VOOPOO electronic cigarette, and (c) 1R6F reference tobacco cigarette. Unshaded and shaded data represent primary and secondhand cigarette aerosols, respectively. Red dashed lines show the maximum intake amount regulated by the European Medicine Agency (10 ng for Ni and 100 ng for Cr).

and compared them against the primary aerosols (Figure 6). Here, in addition to the VOOPOO electronic cigarette, we analyzed the JUUL electronic cigarette. The masses of the heavy metals were normalized to 100 puffs of smoking. It can be seen that a significant amount of heavy metals can be carried by secondhand electronic cigarette aerosols. The Ni and Cr in the secondhand electronic cigarette aerosols



are  $402 \pm 242$  and  $522 \pm 220$  ng for JUUL, and  $241 \pm 132$  and  $1719 \pm 865$  ng for VOOPPOO, which are all above the daily maximum intake amount regulated by the European Medicine Agency (10 ng for Ni and 100 ng for Cr) (Nordberg et al. 2014). We should also note that the mean puff number for electronic cigarette users per day is 163 (Dautzenberg and Bricard 2015), meaning that the emission of heavy metals from secondhand smoke and its potential environmental and health impact may be alarmingly high. The emission of heavy metal from the electronic cigarettes are comparable to that of the tobacco cigarette (Figure 6(c)), highlighting the importance of controlling the emission of secondhand smoke generated from electronic cigarettes.

## Discussion

### Performance of the filter-based simulated respiratory system

In this study, we assembled a filter-based simulated respiratory system that mimics the particle deposition and hygroscopic growth in human lungs. The fabric materials used in the system have a wide range of surface areas, creating particle deposition efficiencies that are similar to different regions of the human respiratory system. In the size range studied (30 to 500 nm), the AL region has the highest deposition efficiency (Figure 3) due to its large surface area and long residence time of the particles, facilitating the deposition of particles by Brownian diffusion. The ET and TB regions have relatively lower particle deposition efficiencies because the primary particle deposition mechanisms in these regions are through impaction and interception, which are insignificant for submicron particles. However, the ET region has an increased deposition efficiency with increasing particle size due to particle deposition by impaction and interception. The filter-based system also has a relatively consistent performance under different flow rates (Supplementary Figure S2).

The size-dependent particle deposition efficiency for tobacco cigarette aerosols follows the NaCl and the ICRP model, whereas the electronic cigarette aerosols differ considerably from the other aerosols (Figure 5). This discrepancy can be explained by the evaporation and transport of the electronic cigarette aerosols in the filter-based system. Although all particles in the filter-based system are subject to hygroscopic growth, the electronic cigarette aerosols are generated as liquid droplets mainly composed of volatile organic buffer liquid, such as propylene glycol (PG) and vegetable glycerin (VG). The characteristic evaporation time of these liquid droplets can be calculated by (Friedlander 1977)

$$\tau_{\text{evap}} = \frac{kTD_p^2}{4Dv_m\chi(p_d - p)} \quad (26)$$

where  $D$  is the diffusivity of the evaporating vapor molecule,  $p$  represents the partial pressure of the vapor and  $p_d$  represents the equilibrium vapor pressure at the surface of the droplet, which is calculated by  $p_d = p_s(T)\exp\left(\frac{4\sigma v_m}{kTD_p}\right)$  (Butt

et al. 2013).  $T$  is the ambient temperature,  $v_m$  is the molar volume of the liquid, and  $\sigma$  represents the surface tension of the liquid.  $\chi$  corrects for the non-continuum effect of the particles, and is calculated using  $\chi = \frac{1+Kn}{1+1.71Kn+1.333Kn^2}$  (Hegg and Larson 1990), where  $Kn$  is the Knudsen number ( $Kn = 2\lambda/D_p$ ,  $\lambda$  is the mean free path of vapor molecules in air). With this equation, we can estimate that it generally requires 0.021 s and 1.7 s for a 500 nm PG and VG droplet to evaporate sufficiently. The large difference between PG and VG droplet evaporation time is due to the relatively low vapor pressure of the VG, which has a value of 0.018 Pa under 25 °C compared to 13.7 Pa for PG (Yaws and Gabbula 2003). Note that smaller particles evaporate even faster because  $\tau_{\text{evap}}$  scales with  $D_p^2$ . The transport time of aerosols in the filter-based system is 0.057 s (tube diameter of 6 mm and tube length of 20 cm at a flow rate of 6 lpm), meaning that the larger droplets containing PG and VG can evaporate sufficiently and shrink into smaller droplets mainly containing VG as they travel through the filter-based system. Because of droplet evaporation, the number concentration of larger particles downstream of the filter-based system becomes lower, leading to an increased deposition efficiency of the larger particles. The evaporated droplets shrink to smaller sizes, increasing the concentration of the smaller particles, which eventually leads to a lower deposition efficiency of these smaller particles. We should note that similar processes occur in the actual human respiratory system due to the similar physical processes of the electronic cigarette aerosols, but with more complicated effects in the actual case. Compared to electronic cigarettes, tobacco cigarettes mainly generate aerosols in the solid phase with low volatility (Meišutovič-Akhtarieva et al. 2021), meaning that these aerosols can remain in their physical sizes or grow due to aerosol hygroscopic behavior during transport within the filter-based system. It is also likely that the hygroscopic growth of the tobacco cigarette aerosols in the filter-based system dominates constituent evaporation. Due to these reasons, the size-dependent particle deposition efficiency for the tobacco cigarette aerosols is similar to that of the NaCl particles and the ICRP model.

Apart from the phase change of the aerosols, the coagulation of the primary aerosols prior to their entrance to the filter-based simulated respiratory system also needs to be estimated. The characteristic coagulation time based on Brownian diffusion can be estimated by (Friedlander 1977)

$$\tau = \frac{3\mu}{4kTN} \quad (27)$$

where  $\mu$  is the air dynamic viscosity,  $k$  is the Boltzmann constant,  $T$  is the temperature, and  $N$  is the total number concentration of aerosols. Assuming  $N = 10^6 \text{ cm}^{-3}$ , which is the upper limit of concentration of primary smoke aerosols, we can estimate the lower limit of the characteristic coagulation time. The lower limit of  $\tau$  is 3400s, which is far longer than the transport time of aerosols in the filter-based system (0.057 s as shown earlier). This means that coagulation of the primary aerosols on particle deposition in the filter-based system can be neglected.

## Metals in secondhand electronic cigarette aerosols

The formation of metal-containing aerosols is a major issue for electronic cigarettes due to the intense heating of the metal filaments for evaporating the vaping fluid (Goniewicz et al. 2014; Mikheev et al. 2016; Olmedo et al. 2018). These filaments are typically made with kanthal or nichrome, containing Zn, Ni, Cr, Cu, Mn, and other heavy metals. These heavy metals can induce cytotoxicity due to the formation of reactive oxygen species and inflammation, and lead to acute or chronic pulmonary and cardiovascular diseases (Layden et al. 2020). Our analyses show that secondhand electronic cigarette aerosols may contain high concentrations of metals, leading to toxicological effects on non-users of electronic cigarettes. One should also note that according to ICRP (1995), the introduction of metal oxides to salt particles may lead to significant changes in aerosol hygroscopicity, further affecting the lung deposition and the generated secondhand smoke aerosols. Therefore, more laboratory studies are needed to understand the release and toxicological profile of these secondhand electronic cigarette aerosols.

## Perspectives

In this study, we established a filter-based simulated respiratory system for secondhand aerosol generation. The system can mimic the particle capture and hygroscopic growth of particles in the human respiratory system, and produce similar size-dependent particle deposition efficiency (the absolute difference is below 10% at all sizes) compared to the ICRP model under a relative humidity of 90%. Thus, the system could generate representative secondhand aerosols for both tobacco and electronic cigarettes. Importantly, with this system, we demonstrated that the heavy metal contents in secondhand electronic cigarette aerosols were comparable to those in the primary aerosols. Such emission of metal- and nicotine-containing aerosols may be a health issue for nonsmokers, who may inadvertently inhale these aerosols.

Future improvements of the filter-based simulated respiratory system will focus on the following aspects: (1) Understanding the dependence of particle deposition and penetration on the chemical composition of the particles. We note that the ICRP model used in this study assumes that particles are composed of NaCl, while the (ICRP 1995) also pointed out that particles of different chemical compositions may show a large variety in the deposition efficiencies due to the different hygroscopic properties. Therefore, the proposed filter-based system in this study is not a 'one-size-fits-all' system, meaning that human subjects are still required to characterize the respiratory deposition. However, this work shows that, by properly choosing the filter media, we could construct a filter-based system that produces particle deposition efficiencies similar to the respiratory system. Given the wide range of filter materials, we could also identify other filter media to mimic the particle deposition when other types of aerosols are examined in the actual human respiratory system. (2) Examining

vapor deposition in the filter-based system. Although we observed how evaporation may affect the particle deposition in the experiments of electronic cigarette aerosols, we need to note that the actual deposition may be different from our observation. Due to the strong dependence of vapor adsorption and absorption on the properties of the deposited surfaces, vapor deposition in simulated respiratory systems (such as the cast and 3D printed systems, together with the filter-based system) and the actual respiratory system can be drastically different. Therefore, human subjects are still required when vapors are involved in analyzing the respiratory deposition. However, the filter-based system can still be constructed and deployed by properly selecting the filter media (using Equations (18) to (20)) to simulate the actual respiratory deposition once it is experimentally determined. Due to its simple structure, the constructed filter-based system can greatly reduce the complexity involved in human subject studies. (3) Combining an air-liquid interface system with the filter-based simulated respiratory system for direct particle deposition onto human lung epithelial cells. Such a combination can enable the toxicological analysis of secondhand electronic cigarette aerosols. The air-liquid interface system can also be installed between stages of the filter-based simulated respiratory system to study the response of different human lung epithelial cells (e.g. cells from ET, TB, or AL regions) to the aerosols. (4) Replacing the fabric materials with standardized filter materials (such as glass fiber filters and Teflon filters with customized fiber diameters and porosities) to effectively extract metal and organic components in different regions of the simulated respiratory system. Such a study could help understand the region-specific deposition patterns of aerosols in the human respiratory system. (5) Modification of the filter-based simulated respiratory system to mimic tidal flow and the pulsation between inhalation and exhalation. The tidal flow- and pulsation-based simulated respiratory system will be closer to the actual lung and will be able to better simulate the deposition and exhaled aerosols. The improvement could also help understand how the user habits may affect the emission of secondhand smoke aerosols, the compartmental deposition fraction, and the associated toxicological effects. (6) Improving the temperature control of the simulated respiratory system so that it operates under a temperature close to human body temperature ( $\sim 37^{\circ}\text{C}$ ).

## Acknowledgments

We appreciate the inputs from Dr. Lung-Chi Chen at the Department of Environmental Medicine, New York University.

## Disclosure statement

No potential conflict of interest was reported by the author(s).

## Data availability

Data are available upon request.

## References

- Andreoli C, Gigante D, Nunziata A. 2003. A review of in vitro methods to assess the biological activity of tobacco smoke with the aim of reducing the toxicity of smoke. *Toxicol In Vitro*. 17(5–6): 587–594.
- Anselm A, Gebhart J, Heyder J, Ferron G. 1986. *Aerosols: formation and reactivity* (vol. 429). Oxford: Pergamon Press; p. 252.
- Asgari M, Lucci F, Bialek J, Dunan B, Andreatta G, Smajda R, Lani S, Blondiaux N, Majeed S, Steiner S, et al. 2019. Development of a realistic human respiratory tract cast representing physiological thermal conditions. *Aerosol Sci Technol*. 53(8):860–870.
- Asgari M, Lucci F, Kuczaj AK. 2021. Multispecies aerosol evolution and deposition in a human respiratory tract cast model. *J Aerosol Sci*. 153:105720.
- Bair W. 1995. The ICRP human respiratory tract model for radiological protection. *Radiat Prot Dosim*. 60:307–310.
- Blanchard JD, Willeke K. 1984. Total deposition of ultrafine sodium chloride particles in human lungs. *J Appl Physiol Respir Environ Exerc Physiol*. 57(6):1850–1856.
- Butt HJ, Graf K, Kappl M. 2013. *Physics and chemistry of interfaces*. John Wiley & Sons.
- Chen X, Feng Y, Zhong W, Kleinstreuer C. 2017. Numerical investigation of the interaction, transport and deposition of multicomponent droplets in a simple mouth-throat model. *J Aerosol Sci*. 105: 108–127.
- Czogala J, Goniewicz ML, Fidelus B, Zielinska-Danch W, Travers MJ, Sobczak A. 2014. Secondhand exposure to vapors from electronic cigarettes. *Nicotine Tob Res*. 16(6):655–662.
- Dautzenberg B, Bricard D. 2015. Real-time characterization of e-cigarettes use: the 1 million puffs study. *J Addict Res Ther*. 6:4172.
- Ferron G. 1977. The size of soluble aerosol particles as a function of the humidity of the air. Application to the human respiratory tract. *J Aerosol Sci*. 8(4):251–267.
- Ferron G, Kreyling W, Haider B. 1988. Inhalation of salt aerosol particles—ii. Growth and deposition in the human respiratory tract. *J Aerosol Sci*. 19(5):611–631.
- Office of the Surgeon General. 2006. *The health consequences of involuntary exposure to tobacco smoke: a report of the surgeon general*. US Department of Health and Human Services, Public Health Service, Office of the Surgeon General.
- Friedlander SK. 1977. *Smoke, dust and haze: fundamentals of aerosol behavior*. New York: Wiley.
- Goniewicz ML, Knysak J, Gawron M, Kosmider L, Sobczak A, Kurek J, Prokopowicz A, Jablonska-Czapla M, Rosik-Dulewska C, Havel C, et al. 2014. Levels of selected carcinogens and toxicants in vapour from electronic cigarettes. *Tob Control*. 23(2):133–139.
- Grinshpun SA, Haruta H, Eninger RM, Reponen T, McKay RT, Lee S-A. 2009. Performance of an n95 filtering facepiece particulate respirator and a surgical mask during human breathing: two pathways for particle penetration. *J Occup Environ Hyg*. 6(10):593–603.
- Hao W, Parasch A, Williams S, Li J, Ma H, Burken J, Wang Y. 2020. Filtration performances of non-medical materials as candidates for manufacturing facemasks and respirators. *Int J Hyg Environ Health*. 229:113582.
- Hao W, Xu G, Wang Y. 2021. Factors influencing the filtration performance of homemade face masks. *J Occup Environ Hyg*. 18(3): 128–138.
- Hegg DA, Larson TV. 1990. The effects of microphysical parameterization on model predictions of sulfate production in clouds. *Tellus B*. 42(3):272–284.
- Heyder J, Gebhart J, Rudolf G, Schiller CF, Stahlhofen W. 1986. Deposition of particles in the human respiratory tract in the size range 0.005–15  $\mu\text{m}$ . *J Aerosol Sci*. 17(5):811–825.
- Hindle M, Longest PW. 2010. Evaluation of enhanced condensational growth (ecg) for controlled respiratory drug delivery in a mouth-throat and upper tracheobronchial model. *Pharm Res*. 27(9): 1800–1811.
- Hinds WC. 1999. *Aerosol technology: properties, behavior, and measurement of airborne particles*. New York: John Wiley & Sons.
- Hoover MD, Stefaniak AB, Day GA, Geraci CL. 2007. Exposure assessment considerations for nanoparticles in the workplace. In *Nanotoxicology*. Boca Raton: CRC Press; pp. 87–100.
- Hussain M, Madl P, Khan A. 2011. Lung deposition predictions of airborne particles and the emergence of contemporary diseases, part-I. *Health*. 2:51–59.
- ICRP. 1995. *Icrp publication 66: human respiratory tract model for radiological protection*. Oxford: Elsevier Health Sciences.
- Kapiamba KF, Hao W, Adom S, Liu W, Huang Y, Wang Y. 2022. Examining the metal contents in primary and secondhand aerosols released by electronic cigarettes. *Chem Res Toxicol*. 2022:1c00411.
- Kaufman P, Dubray J, Soule EK, Cobb CO, Zarins S, Schwartz R. 2018. Analysis of secondhand e-cigarette aerosol compounds in an indoor setting. *Tobacco Reg Sci*. 4(3):29–37.
- Layden JE, Ghinai I, Pray I, Kimball A, Layer M, Tenforde MW, Navon L, Hoots B, Salvatore PP, Elderbrook M, et al. 2020. Pulmonary illness related to e-cigarette use in Illinois and Wisconsin – final report. *N Engl J Med*. 382(10):903–916.
- Lee K, Ramamurthi M. 1993. Willeke K, Baron PA (eds) *aerosol measurement. Principles, techniques, and applications*. Chap 10. New York: Van Nostrand Reinhold.
- Logue JM, Sleiman M, Montesinos VN, Russell ML, Litter MI, Benowitz NL, Gundel LA, Destailhats H. 2017. Emissions from electronic cigarettes: assessing vapers' intake of toxic compounds, secondhand exposures, and the associated health impacts. *Environ Sci Technol*. 51(16):9271–9279.
- Löndahl J, Pagels J, Boman C, Swietlicki E, Massling A, Rissler J, Blomberg A, Bohgard M, Sandström T. 2008. Deposition of biomass combustion aerosol particles in the human respiratory tract. *Inhal Toxicol*. 20(10):923–933.
- Meišutovič-Akhtarieva M, Prasauskas T, Čiužas D, Kaunelienė V, Martuzevičius D. 2021. The dynamics of exhaled aerosol following the usage of heated tobacco product, electronic cigarette, and conventional cigarette. *Aerosol Air Qual Res*. 21:1–15.
- Mikheev VB, Brinkman MC, Granville CA, Gordon SM, Clark PI. 2016. Real-time measurement of electronic cigarette aerosol size distribution and metals content analysis. *Nicotine Tob Res*. 18(9): 1895–1902.
- Morrow PE. 1986. Factors determining hygroscopic aerosol deposition in airways. *Physiol Rev*. 66(2):330–376.
- Nordberg GF, Fowler BA, Nordberg M. 2014. *Handbook on the toxicology of metals*. Amsterdam: Academic Press.
- Nordlund M, Belka M, Kuczaj AK, Lizal F, Jedelsky J, Elcner J, Jicha M, Sauser Y, Le Bouhellec S, Cosandey S, et al. 2017. Multicomponent aerosol particle deposition in a realistic cast of the human upper respiratory tract. *Inhal Toxicol*. 29(3):113–125.
- Normalización O. I. D (ISO). 2000. ISO 3308: 2000-04-15: Routine analytical cigarette-smoking machine—definition and standard conditions. Geneva: International Organization for Standardization.
- Olmedo P, Goessler W, Tanda S, Grau-Perez M, Jarmul S, Aherrera A, Chen R, Hilpert M, Cohen JE, Navas-Acien A, et al. 2018. Metal concentrations in e-cigarette liquid and aerosol samples: the contribution of metallic coils. *Environ Health Perspect*. 126(2):027010.
- Pankow JF. 2001. A consideration of the role of gas/particle partitioning in the deposition of nicotine and other tobacco smoke compounds in the respiratory tract. *Chem Res Toxicol*. 14(11): 1465–1481.
- Pichelstorfer L, Hofmann W. 2015. Modeling aerosol dynamics of cigarette smoke in a denuder tube. *J Aerosol Sci*. 88:72–89.
- Pichelstorfer L, Hofmann W, Winkler-Heil R, Yurteri CU, McAughey J. 2016. Simulation of aerosol dynamics and deposition of combustible and electronic cigarette aerosols in the human respiratory tract. *J Aerosol Sci*. 99:125–132.
- Pichelstorfer L, Winkler-Heil R, Hofmann W. 2013. Lagrangian/eulerian model of coagulation and deposition of inhaled particles in the human lung. *J Aerosol Sci*. 64:125–142.
- Protano C, Manigrasso M, Avino P, Vitali M. 2017. Second-hand smoke generated by combustion and electronic smoking devices used in real scenarios: ultrafine particle pollution and age-related dose assessment. *Environ Int*. 107:190–195.

- Rostami AA. 2009. Computational modeling of aerosol deposition in respiratory tract: a review. *Inhal Toxicol.* 21(4):262–290.
- Schripp T, Markewitz D, Uhde E, Salthammer T. 2013. Does e-cigarette consumption cause passive vaping? *Indoor Air.* 23(1):25–31.
- Seinfeld J, Pandis S. 2008. *Atmospheric chemistry and physics*, 1997. New York: John Wiley & Sons.
- Son Y, Giovenco DP, Delnevo C, Khlystov A, Samburova V, Meng Q. 2020. Indoor air quality and passive e-cigarette aerosol exposures in vape-shops. *Nicotine Tob. Res.* 22(10):1772–1779.
- Tu K, Knutson E. 1984. Total deposition of ultrafine hydrophobic and hygroscopic aerosols in the human respiratory system. *Aerosol Sci Technol.* 3(4):453–465.
- US Department of Health and Human Services. 2014. *The health consequences of smoking—50 years of progress: a report of the Surgeon General*.
- Wang Y, Li J, Leavey A, O’Neil C, Babcock HM, Biswas P. 2017. Comparative study on the size distributions, respiratory deposition, and transport of particles generated from commonly used medical nebulizers. *J Aerosol Med Pulm Drug Deliv.* 30(2):132–140.
- Worth Longest P, Xi J. 2008. Condensational growth may contribute to the enhanced deposition of cigarette smoke particles in the upper respiratory tract. *Aerosol Sci Technol.* 42(8):579–602.
- Xi J, Kim J, Si XA, Zhou Y. 2013. Hygroscopic aerosol deposition in the human upper respiratory tract under various thermo-humidity conditions. *J Environ Sci Health A Tox Hazard Subst Environ Eng.* 48(14):1790–1805.
- Yaws CL, Gabbula C. 2003. *Yaws’ handbook of thermodynamic and physical properties of chemical compounds*. New York: Knovel.
- Yeh H-C, Liu BY. 1974. Aerosol filtration by fibrous filters—I. Theoretical. *J Aerosol Sci.* 5(2):191–204.
- Zhang Y, Sumner W, Chen D-R. 2013. In vitro particle size distributions in electronic and conventional cigarette aerosols suggest comparable deposition patterns. *Nicotine Tob Res.* 15(2):501–508.
- Zhang Z, Kleinstreuer C. 2011. Deposition of naphthalene and tetradecane vapors in models of the human respiratory system. *Inhal Toxicol.* 23(1):44–57.
- Zhang Z, Kleinstreuer C, Feng Y. 2012. Vapor deposition during cigarette smoke inhalation in a subject-specific human airway model. *J Aerosol Sci.* 53:40–60.
- Zhao T, Nguyen C, Lin C-H, Middlekauff HR, Peters K, Mohemani R, Guo Q, Zhu Y. 2017. Characteristics of secondhand electronic cigarette aerosols from active human use. *Aerosol Sci Technol.* 51(12):1368–1376.
- Zhou Y, Sun J, Cheng Y-S. 2011. Comparison of deposition in the usp and physical mouth-throat models with solid and liquid particles. *J Aerosol Med Pulm Drug Deliv.* 24(6):277–284.